Tuo *et al. Chem. Synth.* **2025**, *5*, 53
DOI: 10.20517/cs.2024.194

Chemical Synthesis

Research Article

Open Access

Selective syngas conversion to olefins over bifunctional $Zn_2Al_3O_4$/PLS-3 catalyst

Jie Tuo[1], Xianchen Gong[1], Zhenteng Sheng[1], Qi Yang[1], Hao Xu[1,2,*], Yejun Guan[1,2], Peng Wu[1,2,*]

[1]State Key Laboratory of Petroleum Molecular & Process Engineering, Shanghai Key Laboratory of Green Chemistry and Chemical Processes, School of Chemistry and Molecular Engineering, East China Normal University, Shanghai 200062, China.
[2]Institute of Eco-Chongming, Shanghai, 202162, China.

[*]**Correspondence to:** Prof. Hao Xu, Prof. Peng Wu, State Key Laboratory of Petroleum Molecular & Process Engineering, Shanghai Key Laboratory of Green Chemistry and Chemical Processes, School of Chemistry and Molecular Engineering, East China Normal University, No. 3663 North Zhongshan Road, Shanghai 200062, China. E-mail: hxu@chem.ecnu.edu.cn; pwu@chem.ecnu.edu.cn

How to cite this article: Tuo, J.; Gong, X.; Sheng, Z.; Yang, Q.; Xu, H.; Guan, Y.; Wu, P. Selective syngas conversion to olefins over bifunctional $Zn_2Al_3O_4$/PLS-3 catalyst. *Chem. Synth.* **2025**, *5*, 53. https://dx.doi.org/10.20517/cs.2024.194

Received: 11 Nov 2024 **First Decision:** 25 Jan 2025 **Revised:** 16 Feb 2025 **Accepted:** 22 Feb 2025 **Published:** 23 May 2025

Academic Editor: Ren-Hua Jin **Copy Editor:** Pei-Yun Wang **Production Editor:** Pei-Yun Wang

Abstract

Designing zeolites with novel topologies and tunable acidity to construct metal oxide-zeolite bifunctional catalytic systems for targeted transformation of syngas into high-value olefins has aroused wide interest. PLS-3 aluminosilicates with the **FER** topology and unique nanorod crystal morphology, derived from layered precursors with a wide Si/Al ratio range of 50-300, were applied to combine with $Zn_2Al_3O_4$ oxide, constructing bifunctional catalysts for selective syngas conversion reaction. The lower Al content in PLS-3 zeolite led to decreased acid amount and the preferred distribution of framework Al atoms in specific tetrahedral locations (T2 and T4), which promoted the formation of ethylene. High-silica PLS-3 (Si/Al = 250) combined with $Zn_2Al_3O_4$ oxide showed high selectivity for $C_{2-5}^{=}$ (78.5%), especially for ethylene (45%), and high ratios of ethylene to propylene (*E/P*, 7.0) and olefin to paraffin (*O/P*, 21.2). Furthermore, the *in-situ* infrared spectra evidenced that the syngas conversion over $Zn_2Al_3O_4$/PLS-3 catalyst possibly followed the carbonylation route.

Keywords: PLS-3 zeolite, bifunctional catalyst, olefins, syngas conversion

INTRODUCTION

Syngas conversion is an effective process that converts non-petroleum carbon-based resources, such as coal, natural gas, and biomass, into high-value hydrocarbon chemicals[1-3]. The precise regulation of product

distribution is a great challenge in traditional Fischer-Tropsch synthesis (FTS) process because the product distribution follows the Anderson-Schulz-Flory (ASF) model. Light olefins are important basic chemical raw materials, and thus the selective conversion of syngas to light olefins has become a research hotspot[4,5]. The Fe, Co, Ni, and Ru metals as main catalysts of FTS process have been extensively studied, but their light hydrocarbon selectivity did not exceed 58%. The supported iron nanoparticles and cobalt carbide nanoprisms were prepared by the regulation of metal morphology, and the high selectivity of light olefins up to 60% could be achieved, breaking the ASF distribution[6,7]. Furthermore, the bifunctional catalyst was also developed for the syngas conversion reaction by combining the FTS metal with zeolites, where zeolites with distinctive shape-selectivity and tunable acidity can shear the long-chain hydrocarbons to realize the high selectivity of light olefin[8-10]. However, the selectivity of light olefins still is low on traditional FTS process.

In 2016, the syngas direct conversion into light olefins was achieved by coupling the methanol synthesis and methanol to olefins (MTO) process using the bifunctional catalysts of metal oxides ($ZnCrO_x$, $ZnZrO_x$, and $ZnAlO_x$) combined with the SAPO-34 zeolite[11-13]. The composited catalyst system of metal oxide–zeolite greatly broke the ASF limitation of syngas conversion, and the light olefin selectivity reached as high as 80%, far exceeding that of the conventional FTS process. The activation of CO and facilitation of C–C coupling is critical for syngas conversion, and the CH_2CO (ketene) and/or CH_3O^* (methoxy) species have been confirmed as intermediates by activating CO^* and H_2 (or H^*) species over metal oxide[11-13]. For the ketene intermediate route, the protonation of ketene leads to the formation of CH_3CO species, which act as methylating agents toward hydrocarbon pool in SAPO-34 zeolite[14], and then higher olefins or the corresponding carbenium ions obtained by the methylation of olefins with ketene might be cracked into light olefins. In addition, for methanol as an intermediate in the syngas conversion, the hydrocarbon pool mechanism of MTO has been widely accepted[15]. Recently, the methanol carbonylation route to acetic acid (AA) followed by the selective conversion of AA to ethylene was proposed over bifunctional catalyst for the methanol conversion in syngas[16].

The metal oxide components result in the difference of intermediates, such as ketene and methanol, while zeolite is responsible for the intermediate conversion to obtain the target product for the oxide-zeolite catalyzed syngas conversion[11-13]. The topology, pore structure and acidity of zeolite synergistically affect the product distribution in the metal oxide-zeolite bifunctional catalyst system. The small-pore zeolites with the **CHA** (SAPO-34 and SSZ-13) and **AEI** (SAPO-18 and AlPO-18) topologies both gave the main hydrocarbon products of light olefins[17-21]. Wang *et al.* found that different product distributions in a range of light olefins were obtained using 8-ring (R) small-pore zeolites with different cavities and topologies, such as SAPO-17 (**ERI**), SAPO-34 (**CHA**) and SAPO-18 (**AEI**)[22]. Ethylene (32%) and methane (13%) were main products over $ZnAlO_x$/SAPO-17, while $ZnAlO_x$/SAPO-34 mainly produced propylene (48%) and ethylene (23%). $ZnAlO_x$/SAPO-18 with large cages also mainly produced propylene (38%) followed by butene with selectivity of 20%. In a particular case, a high ethylene selectivity of 73% was obtained over the $ZnCrO_x$ combined with 12R large-pore **MOR** zeolite in the syngas conversion reaction, in which the acid sites within 12R pores were selectively poisoned by pyridine, making the reaction take place restrictedly within the narrow space of 8R side pockets[23]. These results indicated that the cage-type small-pore zeolites favor the formation of light olefins due to the spatial confinement effect unfavorable for C–C coupling. In addition to zeolite topology, the acid property can also affect the product distribution of syngas conversion. AlPO-18 zeolite with weaker acidity showed a higher olefin/paraffin (*O/P*) ratio than that of SAPO-34 when combined with $ZnCrO_x$ and applied in the syngas conversion reaction[19].

Jiao *et al.* also found that the Ge-substituted AlPO-18 zeolite with $ZnCrO_x$ gave a $C_{2-4}^{=}$ selectivity of 83% in syngas conversion reaction, which is due to the weaker acidity of Ge(OH)Al group in comparison to that of Si(OH)Al[24]. Recently, we combined Al-IDM-1 (**-ION**) zeolite with $Zn_aAl_bO_x$ oxide to catalyze the syngas conversion reaction, showing a $C_{3-4}^{=}$ selectivity of 88% in light olefins and a high *O/P* ratio of 14[25]. We demonstrated that the Al-IDM-1 zeolite exhibited weak acidity, thus enhancing the olefin-based cycle and promoting $C_{3-4}^{=}$ formation. These studies indicated that the weakened acidity has been proven to favor the formation of light olefins. Thus, the usage of zeolites with suitable pore structure and acidity to catalyze the conversion of syngas by combining with metal oxide is crucial to achieve specific olefins.

The **FER** zeolite consists of 8R (3.5 × 4.8 Å) and 10R (4.2 × 5.4 Å) pore channels along the *b*- and *c*-axes, respectively, which proves to be active in the reactions of 1-butene isomerization and carbonylation of dimethyl ether (DME)[26,27]. Similar to **MOR** zeolite, **FER** zeolite has the potential for selective conversion of syngas to olefins by making full use of its 8R pores. Herein, the PLS-3 zeolites with different Si/Al ratios, derived from a lamellar precursor with a structure similar to PREFER, were synthesized to catalyze the syngas conversion reaction by combining with $Zn_2Al_3O_4$ oxide. The effect of zeolite acidity and reaction conditions on the catalytic performances was investigated in detail in the syngas conversion. In addition, the syngas conversion mechanism over the $Zn_2Al_3O_4$/PLS-3 catalyst was also studied via the *in-situ* infrared (IR) spectra. PLS-3 with suitable acidity was highly selective to the production of olefins, especially ethylene.

EXPERIMENTAL

Synthesis of PLS-3 zeolite

PLS-3 zeolites were synthesized using tetraethylammonium hydroxide solution (TEAOH) and H-kanemite as the structure-directing agent (SDA) and silica source, respectively, according to a previously reported method (Experimental details in Supplementary Materials)[28]. Typically, H-kanemite, NaOH, and $Al(NO_3)_3{\cdot}9H_2O$ were added into the TEAOH solution, and then the solution was stirred for 30 min, resulting in the initial gels with molar compositions of 1.0 SiO_2 : *x*/2 Al_2O_3 : 0.04 NaOH : 0.2 TEAOH : 6.5 H_2O. The synthetic gel was crystallized at 443 K for 6 h, and then the products were collected by filtration, washing, and drying at 373 K for 12 h. The occluded organic species were removed by air calcination at 823 K for 6 h. The PLS-3 zeolite was ion-exchanged with NH_4Cl solution (1 M, the mass ratio of solid/liquid = 1:50) for 3 h at 353 K, and the process was repeated three times. Then, the sample was further calcined at 823 K for 6 h to obtain proton-form PLS-3 zeolites, denoted as PLS-3-*x*, where *x* is the Si/Al ratio in the synthetic gel.

Catalytic reactions

The syngas conversion reaction was tested using a high-pressure fixed-bed stainless steel reactor (inner diameter, 9 mm). For the preparation of the composite catalyst, the $Zn_2Al_3O_4$ and PLS-3-*x* zeolite powders were pressed, crushed, and sieved to 20-40 mesh granules separately. Then, the granules of the two components were physically mixed. Typically, 0.25 g composite catalyst with a metal oxide to zeolite mass ratio of 3:2 was used. The catalyst was pretreated using N_2 (30 $mL{\cdot}min^{-1}$) at a temperature of 673 K for 2 h, cooled to 623 K, and then the N_2 gas was switched to syngas (volume ratio, 1/1; 6,000 $mL{\cdot}g^{-1}{\cdot}h^{-1}$) with the reaction pressure adjusted to 1 MPa. Subsequently, the reaction began after achieving the target temperature, and an online gas chromatograph, equipped with PLOT/Q capillary column (30 m × 0.32 mm × 20 μm) connected to a flame ionization detector (FID) detector and MS-13X column connected to a thermal conductivity detector (TCD) detector, was used to analyze the products. Notably, 4% Ar was used as an inner standard in the syngas flow. The CO conversion, along with CO_2 and hydrocarbon selectivity (C_nH_m), with CO_2 and DME excluded from the hydrocarbon selectivity calculation, was calculated.

The CO conversion [X(CO)] is given by

$$X(\mathrm{CO}) = (1 - \frac{A_{CO}^{out}/A_{Ar}^{out}}{A_{CO}^{in}/A_{Ar}^{in}}) \times 100\%$$

Where A_{CO}^{out} and A_{Ar}^{out} are peak areas of CO and Ar determined by the TCD detector at the outlet, A_{CO}^{in} and A_{Ar}^{in} are peak areas of CO and Ar determined by the TCD detector at the inlet.

The CO_2 selectivity [$S(CO_2)$] is given by

$$S(\mathrm{CO_2}) = \frac{A_{CO_2}/A_{Ar}^{out} \times f_{CO_2}}{(A_{CO}^{in}/A_{Ar}^{in} - A_{CO}^{out}/A_{Ar}^{out}) \times f_{CO}}$$

Where A_{CO_2} is the peak area of CO_2 determined by the TCD detector at the outlet, and f_{CO_2} and f_{CO} are the calibration factors of CO_2 and CO, respectively.

The hydrocarbon selectivity is given by

$$S_i = \frac{A_i \times f_i}{\sum_{i=1}^{max} A_i \times f_i} \times 100\%$$

Where A_i is peak area of specific product i determined via the FID, and f_i is its calibration factor.

RESULTS AND DISCUSSION

Textural properties of PLS-3 zeolites

The as-made PLS-3 zeolite, synthesized with layered silicate H-kanemite as a silica source, showed the X-ray diffraction (XRD) patterns similar to a typical **FER**-type layered zeolite PREFER [Supplementary Figure 1][28]. The layer-related [200] diffraction peak of as-made PLS-3 zeolite shifted from 7.6° to 9.7° after calcination at temperature of 823 K for 6 h, due to the removal of occluded TEA organic species accompanied by the condensation of hydroxyl groups on the neighboring layers, leading to a topotactic transformation from 2D layer structure to 3D **FER** topology, as shown in Supplementary Figure 2. Figure 1A shows the XRD patterns of proton-type PLS-3 zeolites in calcined form with different Si/Al ratios by adjusting Al content in initial synthetic gels. The diffraction peaks corresponding to **FER** zeolite were well-resolved, and impurity phase was absent for all samples, indicating that highly crystalline PLS-3 zeolites were successfully synthesized with different Al amounts. The N_2 sorption isotherms were further measured to characterize the textural properties of PLS-3 zeolites [Figure 1B and Table 1]. The PLS-3 zeolites with different Si/Al ratios showed typical type-I isotherms, indicative of micropore materials. Meanwhile, the adsorbed N_2 amount dramatically raised at high relative pressure region of P/P_0 > 0.8, indicating that PLS-3 zeolite had abundant inter-crystal mesopores. The micropore surface area and volume were ~300 $m^2 \cdot g^{-1}$ and ~0.13 $cm^3 \cdot g^{-1}$ for all PLS-3 zeolites, respectively. The external surface area (~100 $m^2 \cdot g^{-1}$) and mesopore volume (~0.50 $cm^3 \cdot g^{-1}$) were higher than those of traditional **FER** zeolite with a bulk crystal morphology. Figure 2 showed that the rod-like crystal morphology with a short length of 50 nm was observed for all the PLS-3 zeolites, which is different from that of conventional FER with bulky crystal

Table 1. Textural and physicochemical properties of PLS-3 zeolites with different Si/Al ratios

Sample	Si/Al[a]	S_{BET}[b] ($m^2 \cdot g^{-1}$)	S_{micro}[c] ($m^2 \cdot g^{-1}$)	S_{ext}[d] ($m^2 \cdot g^{-1}$)	V_{total}[e] ($cm^3 \cdot g^{-1}$)	V_{micro}[f] ($cm^3 \cdot g^{-1}$)	V_{meso}[g] ($cm^3 \cdot g^{-1}$)
PLS-3-50	40	425	309	116	0.60	0.14	0.46
PLS-3-100	82	409	297	112	0.66	0.12	0.54
PLS-3-200	95	406	314	92	0.62	0.13	0.49
PLS-3-250	140	403	308	95	0.67	0.13	0.54
PLS-3-300	190	404	303	101	0.67	0.12	0.55
FER	-	390	370	20	0.27	0.14	0.13

[a]Determined by ICP analysis; [b]Total surface area was calculated by BET equation; [c]Micropore surface area; [d]External surface area was calculated by *t*-plot method; [e]Total pore volume was determined at P/P_0 = 0.99; [f]Micropore volume was calculated by *t*-plot method; [g] Mesopore volume was calculated by $V_{meso} = V_{total} - V_{micro}$. ICP: Inductively coupled plasma; BET: Brunauer–Emmett–Teller.

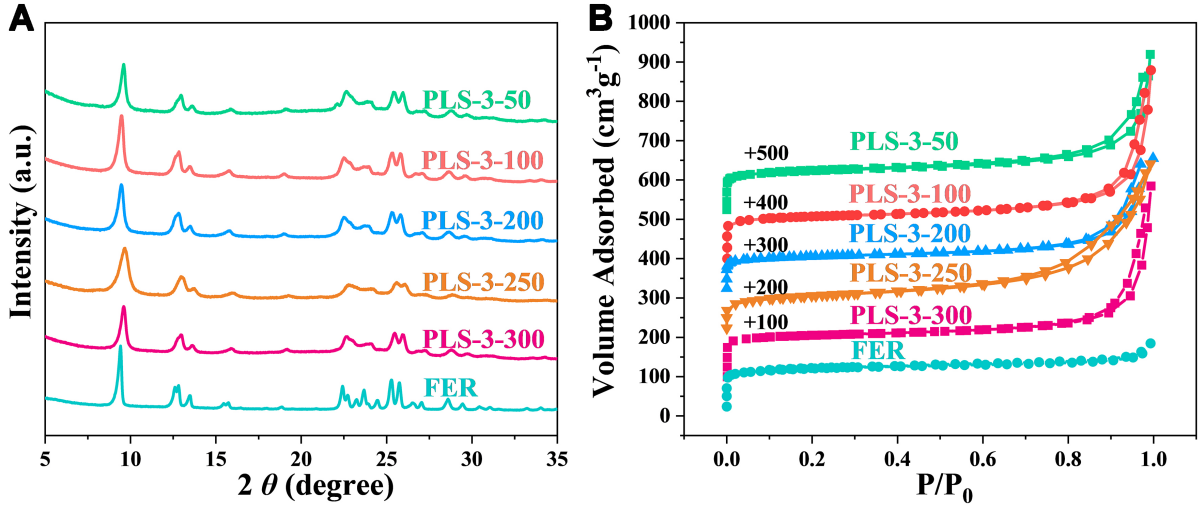

Figure 1. The (A) XRD patterns and (B) N_2 sorption isotherms of PLS-3 zeolites with different Al contents. XRD: X-ray diffraction.

morphology [Supplementary Figure 3]. The crystal length of PLS-3 zeolite gradually reduced along with increasing Si/Al ratios.

Acidity of PLS-3 zeolites

The acidity of PLS-3 zeolites with different Si/Al ratios was analyzed via the ^{27}Al magic angle spinning nuclear magnetic resonance (MAS NMR), hydroxyl infrared spectroscopy (OH-IR) and pyridine-adsorption infrared spectroscopy (Py-IR), and NH_3-temperature-programmed desorption (TPD) techniques. The ^{27}Al MAS NMR spectra of PLS-3-*x* samples are shown in Figure 3A. The resonance peaks at 53 and 0 ppm are related to the tetrahedrally coordinated framework Al (Al_F) and the extra-framework Al (EFAl), respectively[29-32]. Nearly all the Al atoms were tetrahedrally coordinated in the framework, showing a strong peak centered at 53 ppm, and the intensity was significantly weakened with the decrease of Al content. In addition, the peak corresponding to Al_F gradually shifted to a higher field with chemical shift changing from 53.7 to 52.7 ppm with decreasing Al amount, indicating that the chemical environment of Al_F changed with the variation of Al content. There are four different tetrahedral (T) sites for the framework Al in **FER** topology. The T1/T2 sites are distributed in the intersection of 10R and 8R pores [Supplementary Scheme 1] while T3 sites are located in the 10R pores. T4 sites situated in 6R pockets can be accessed only through 8R pores[26]. Hence, the peak at 53 ppm was further deconvoluted into four peaks at 60.5, 51, 53.5, and 56.6 ppm to identify the different chemical environment of Al in PLS-3 [Supplementary Figure 4 and

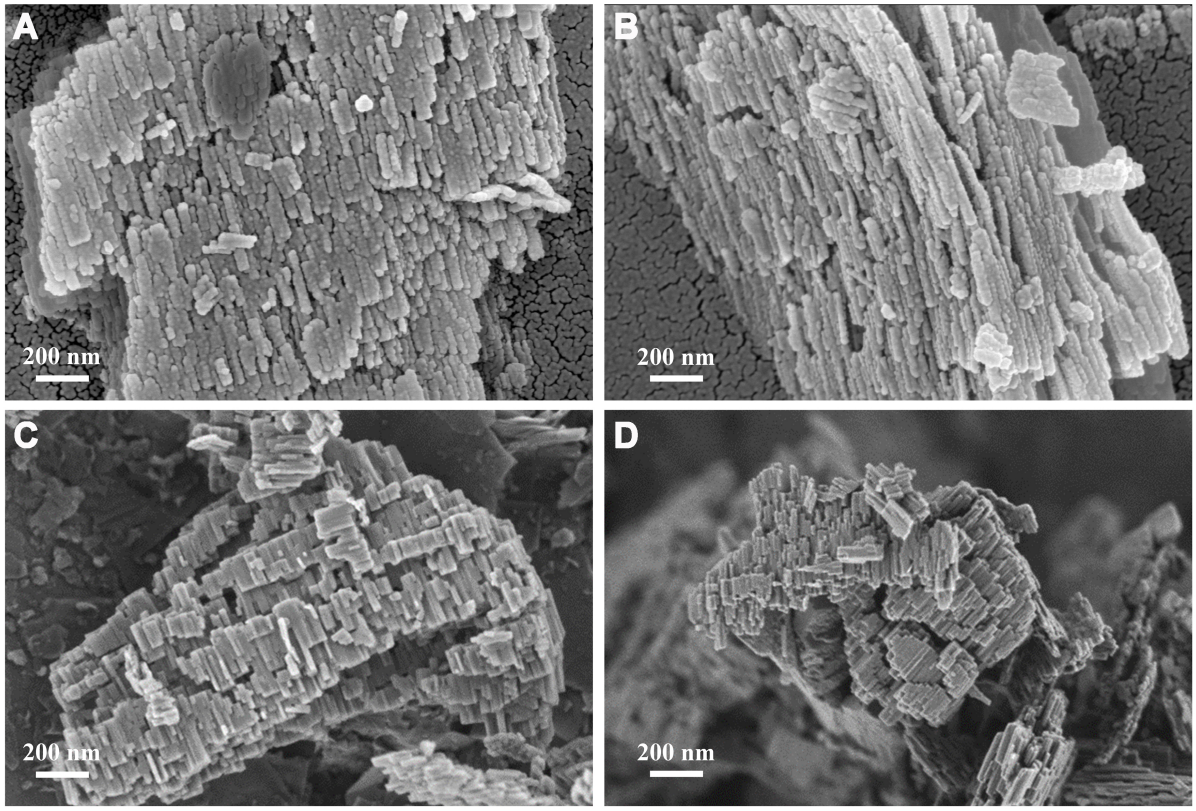

Figure 2. SEM images of (A) PLS-3-50, (B) PLS-3-100, (C) PLS-3-200 and (D) PLS-3-250. SEM: Scanning electron microscope.

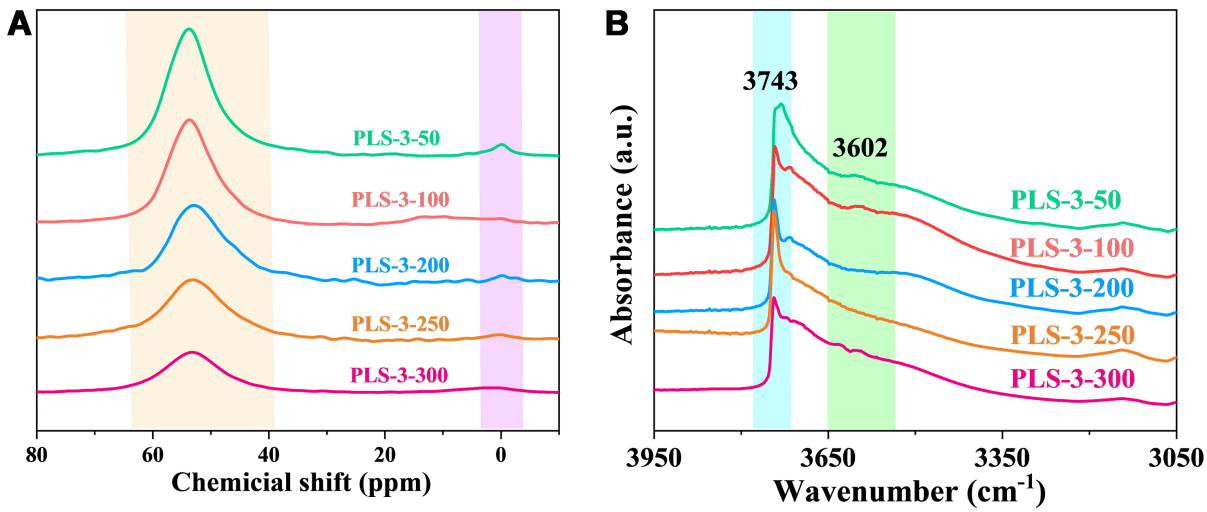

Figure 3. (A) ^{27}Al MAS NMR spectra and (B) IR spectra in the hydroxyl-stretching region of PLS-3 zeolites with different Al contents. MAS NMR: Magic angle spinning nuclear magnetic resonance; IR: infrared.

Table 2], which are related to framework Al sited in T1, T2, T3 and T4, respectively[26]. The Al_F species in T2 sites gradually increased from 40.5% to 68.5% with increasing Si/Al ratio. The proportion of Al_F in T4 sites rose from 15.1% to 22.5% with the Si/Al ratio of 50-200, and then slightly reduced to 18.7% when increasing the Si/Al ratio to 250. However, the percentage in T3 sites decreased from 38.2% to 11.5%. The results

Table 2. Framework Al distributions in different PLS-3 zeolites achieved via the deconvolution of ^{27}Al MAS NMR spectra

Zeolite	T1 (60.5 ppm)	T2 (51.0 ppm)	T3 (53.5 ppm)	T4 (56.6 ppm)
PLS-3-50	6.2	40.5	38.2	15.1
PLS-3-100	2.5	53.7	26.0	17.8
PLS-3-200	3.2	61.8	12.5	22.5
PLS-3-250	1.5	68.3	11.5	18.7

MAS NMR: Magic angle spinning nuclear magnetic resonance.

proved that the spatial distribution of Al_F sites can be tuned by the regulation of the Si/Al ratio in PLS-3 zeolite, and Al_F preferred to locate in T2 and T4 sites at relatively low Al content.

The acidity in PLS-3 zeolites was further investigated by hydroxyl-stretching IR spectra [Figure 3B]. Two main absorption bands were observed at 3,743 and 3,602 cm^{-1}, which are attributed to the terminal Si–OH and the bridging hydroxyl groups (Si–OH–Al), respectively. [25] The intensity of Si–OH–Al groups gradually decreased with increasing Si/Al ratio, in consistent with ^{27}Al MAS NMR spectra. Furthermore, NH_3-TPD curves give the acid amount in PLS-3 zeolites [Figure 4A and Table 3]. The NH_3-TPD curves show two desorption peaks at relatively low (about 423 K) and high temperatures (about 573 K), which are generally attributed to the desorption of NH_3 on weak acid sites (WAS) and strong acid sites (SAS), respectively. The amounts of WAS and SAS also dropped from 142 and 88 μmol·g^{-1} to 20 and 28 μmol·g^{-1}, respectively, with the Si/Al ratio increased from 50 to 300. Moreover, the Py-IR spectra were used to analyze the content of Lewis acid site (LAS) and Brønsted acid site (BAS) after the desorption of physically adsorbed pyridine at 423 K [Figure 4B and Table 3]. The bands at 1,543 and 1,455 cm^{-1} correspond to BAS and LAS, respectively[33]. The band at ~1,490 cm^{-1} is attributed to both BAS and LAS, and the band at 1,445 cm^{-1} is due to hydrogen-bonded pyridine. The contents of BAS and LAS were dramatically reduced with increasing Si/Al ratio, consistent with NH_3-TPD results.

Catalytic performance of syngas conversion

The PLS-3-*x* zeolites were mixed with $Zn_2Al_3O_4$ oxide to catalyze the syngas conversion reaction. The acidity of PLS-3 zeolites could be tuned by varying framework Al content, and the effect of acidity on the product selectivity was further studied by physically mixing PLS-3-*x* zeolites with $Zn_2Al_3O_4$ under the reaction condition at a space velocity of 6,000 mL·g^{-1}·min^{-1}, 623 K, and 1.0 MPa. As shown in Figure 5 and Table 4, the Si/Al ratio of PLS-3 zeolite had little effect on the CO conversion and the CO_2 selectivity, which remained almost unchanged. The selectivity of ethylene dramatically increased from 23.2% to 45.0%, but C_6^+ and C_{2-5}^0 selectivity decreased with increasing the Si/Al ratio from 50 to 250, thus leading to evidently increased *E/P* and *O/P* ratios from 3.6 to 7.0 and from 4.5 to 21.2, respectively. However, the catalytic performance became worse for sample PLS-3-300, showing the high CH_4 selectivity of 12.5% and DME selectivity of 3.1%, due to the difficulty in transforming intermediates over insufficient acid sites. Therefore, using PLS-3-250 as zeolite component combined with $Zn_2Al_3O_4$ oxide gave the optimal catalytic performance in the syngas conversion reaction, that is high selectivity of $C_{2-5}^=$ (78.5%) and ethylene (45%) and high *E/P* (7.0) and *O/P* (21.2) ratios, which breaks the ASF distribution [Supplementary Figure 5]. Moreover, the bifunctional $Zn_2Al_3O_4$/PLS-3 catalysts for syngas conversion have a higher selectivity of ethylene, *O/P* and *E/P* ratio with comparison to the SAPO-type zeolite-based catalysts [Supplementary Table 1]. We speculated that the PLS-3 zeolite with fewer acid sites and more Al_F sited in the T2/T4 sites at a lower Al content may suppress the hydrogen transfer and aromatization reactions, thus leading to the high $C_{2-5}^=$ and ethylene. These results indicated that the acidity of PLS-3 zeolite significantly affected the product selectivity of syngas conversion reaction. Furthermore, the CO conversion and product selectivity were not significantly changed within 100 h over $Zn_2Al_3O_4$/PLS-3-250 catalyst [Figure 6], indicating that this catalyst

Table 3. The acid amounts of PLS-3 zeolites with different Si/Al ratios

Sample	WAS[a] (μmol·g^{-1})	SAS[b] (μmol·g^{-1})	BAS[c] (μmol·g^{-1})	LAS[c] (μmol·g^{-1})
PLS-3-50	142	88	118	47
PLS-3-100	96	82	90	21
PLS-3-200	46	53	60	16
PLS-3-250	31	33	41	11
PLS-3-300	20	28	18	3

[a]WAS was obtained by NH_3-TPD in temperature region of 393-573 K; [b]SAS was obtained by NH_3-TPD in temperature region of 623-823 K; [c]BAS and LAS were determined by Py-IR spectra at 423 K. WAS: Weak acid sites; SAS: strong acid sites; BAS: Brønsted acid site; LAS: Lewis acid site; TPD: temperature-programmed desorption; Py-IR: pyridine-adsorption infrared spectroscopy.

Table 4. Catalytic activity of various $Zn_2Al_3O_4$/PLS-3 catalysts in syngas conversion reaction

Sample	CO conv. (%)	CO_2 sel. (%)	Product distribution (%)					DME (%)	*E/P*	*O/P*
			CH_4	$C_2^=$	$C_{2-5}^=$	C_{2-5}^0	C_6^+			
PLS-3-50	11.1	28.1	4.6	23.2	57.6	12.9	24.9	-	3.6	4.5
PLS-3-100	10.9	22.4	5.3	25.6	60.7	9.9	24.1	-	4.1	6.2
PLS-3-200	10.9	28.7	7.0	29.2	67.5	4.1	21.4	-	5.9	16.3
PLS-3-250	11.0	24.7	6.6	45.0	78.5	3.7	11.2	-	7.0	21.2
PLS-3-300	8.9	24.4	12.5	36.0	68.9	7.6	11.0	3.1	6.1	9.1

DME: Dimethyl ether; *E/P*: ethylene to propylene; *O/P*: olefin to paraffin.

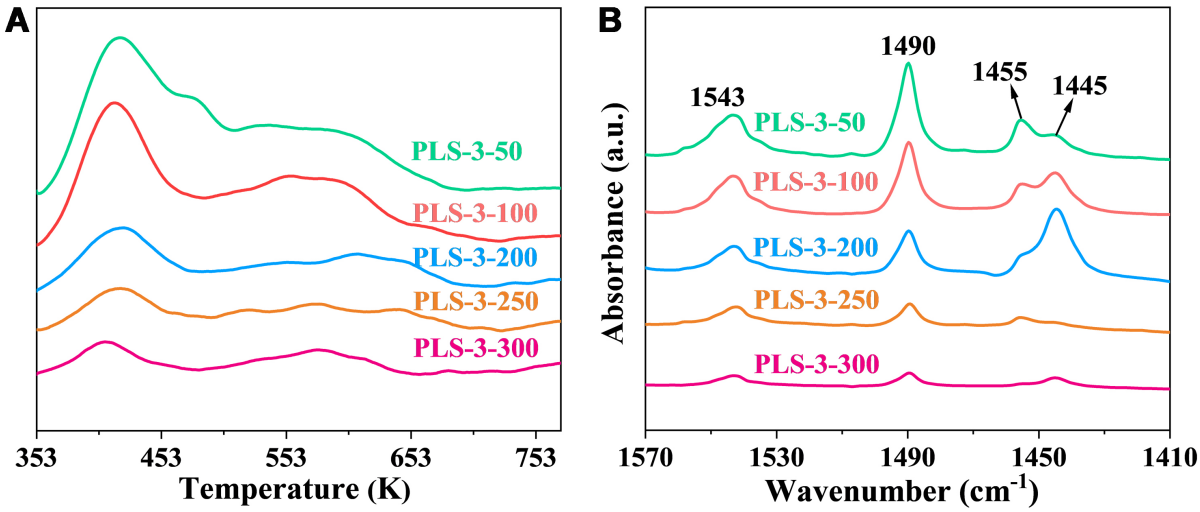

Figure 4. (A) NH_3-TPD curves and (B) Py-IR spectra of PLS-3 zeolites with different Si/Al ratios. Py-IR spectra were measured after desorption of pyridine at 423 K. TPD: Temperature-programmed desorption; Py-IR: pyridine-adsorption infrared spectroscopy.

was durable. However, the catalytic performance gradually decreased after 100 h, accompanied by a significant increase in methane selectivity and a dramatic reduction in ethylene and $C_{2-5}^=$ selectivity.

As shown in Supplementary Figures 6-8 and Supplementary Table 2, we investigated the effects of reaction conditions of weight hourly space velocity (WHSV), temperature, and proximity between two components on the syngas conversion performance using the bifunctional catalysts composed of $Zn_2Al_3O_4$ and PLS-3-250. Increasing the WHSV of syngas from 3,000 to 7,200 mL·g^{-1}·h^{-1} [Supplementary Figure 6 and

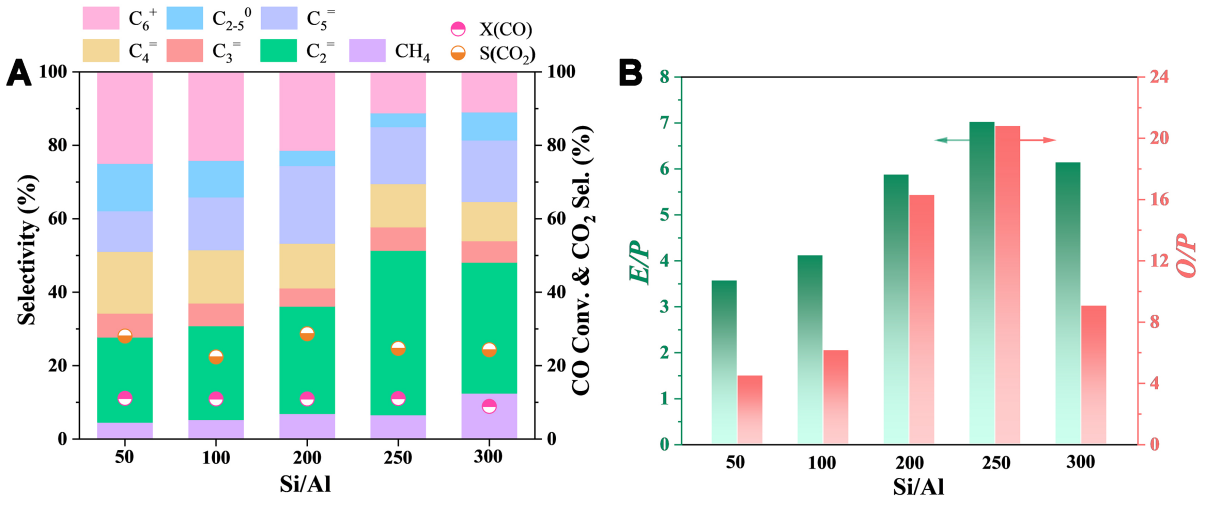

Figure 5. (A) Effect of Si/Al ratio of PLS-3 on the catalytic performance of $Zn_2Al_3O_4$/PLS-3-*x* for syngas conversion; (B) Dependence of *E/P* and *O/P* ratios on the Si/Al ratio of PLS-3. Reaction conditions: catalyst, 0.25 g; metal oxide/zeolite mass ratio, 3:2; temperature, 623 K; pressure, 1 MPa; the WHSV of syngas (H_2/CO volume ratio = 1:1), 6,000 mL·g^{-1}·h^{-1}; TOS, 10 h. *E/P*: Ethylene to propylene; *O/P*: olefin to paraffin; WHSV: weight hourly space velocity; TOS: time on stream.

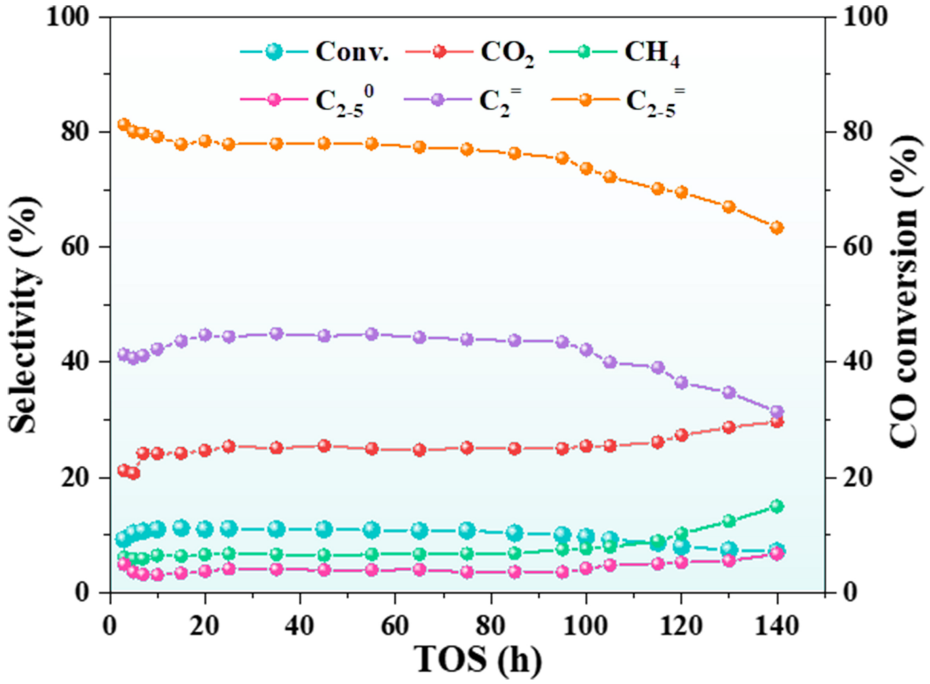

Figure 6. CO conversion and product selectivity with TOS over the bifunctional composite catalyst of $Zn_2Al_3O_4$/PLS-3-250. Reaction conditions: see Figure 5. TOS: Time on stream.

Supplementary Table 2], the CO conversion was decreased (from 13.3% to ~11%) and the selectivity of ethylene (from 29% to >40%) dramatically increased, while the selectivity of C_{2-5}^{0} and C_6^+ was reduced. Among the hydrocarbon products, the *E/P* (from 5.4 to 7.1) and *O/P* (from 16.1 to 23.6) ratios also increased with WHSV. However, the selectivity of long-chain olefins (such as the butene and pentene) was reduced with increasing the WHSV [Supplementary Figure 6A], and they were produced from the ethylene

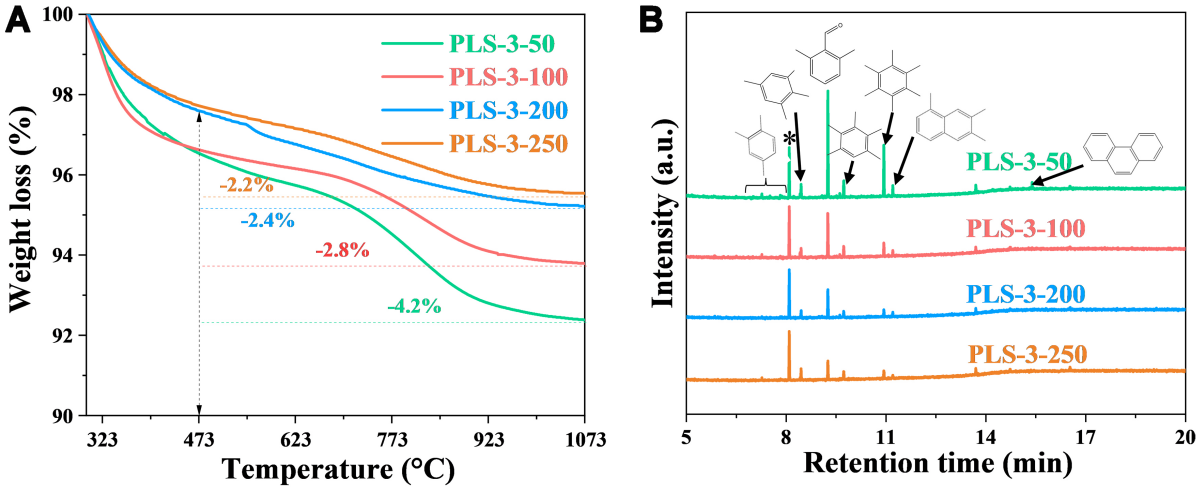

Figure 7. (A) TG curves and (B) GC-MS analysis of the hydrocarbons on the spent catalysts. *The internal standard. TG: Thermogravimetry; GC-MS: gas chromatography-mass spectrometry.

oligomerization reaction. These results indicated that increasing the WHSV of syngas promoted the diffusion of olefin products, which depressed the further hydrogen transfer and ethylene oligomerization to form the alkanes and long-chain hydrocarbons. The reaction temperature showed a more significant effect on the catalytic performance of $Zn_2Al_3O_4$/PLS-3-250 in the syngas conversion reaction [Supplementary Figure 7 and Supplementary Table 2]. The CO conversion and CO_2 selectivity increased with temperature from 603 to 663 K. Furthermore, the higher methane (20.6%) and DME (1.2%) selectivity were observed at a lower temperature of 603 K. The result indicated that the lower temperature is unfavorable for the conversion of methanol intermediate. Meanwhile, the selectivity of C_6^+ exhibited a volcanic trend. At a lower temperature (603 K), the difficulty in converting methanol intermediates led to high CH_4 selectivity but low C_6^+ selectivity, while at higher temperatures (663 K), the suppression of chain growth reactions resulted in low C_6^+ selectivity. In addition, when the temperature was increased from 623 to 663 K, the CH_4 and C_{2-5}^0 were promoted, but $C_{2-5}^=$ and ethylene selectivity were reduced as a result of the enhancement of hydrogen transfer reactions at higher temperatures[3,5], resulting in the highest *E/P* (7.0) and O/P (21.2) ratios at 623 K. With comprehensive consideration of selectivity and conversion, the optimal reduction temperature was 623 K.

In addition, the proximity between two components of zeolite and metal oxide was reported to affect the product distribution in previous studies[5,25]. We thus compared the catalytic performance among three integration manners, including dual bed, granule mixing and mortar mixing [Supplementary Figure 8 and Supplementary Table 2]. Over a dual-bed configuration with PLS-3-250 zeolite downstream from $Zn_2Al_3O_4$ oxide, a lower $C_{2-5}^=$ (33.3%) and ethylene (11%) selectivity but a higher CO_2 (~44%) and CH_4 (~34%) selectivity were observed at low CO conversion (6.7%), and the *E/P* and *O/P* ratios were only 2.0 and 2.2, respectively. For the granule stacking mode, a higher $C_{2-5}^=$ selectivity (78.5%), a higher ethylene selectivity (45%) in olefins, and a lower selectivity of CO_2 (24%) were achieved at CO conversion of 11%. The powder of metal oxide and zeolite was mixed and then compressed into pellets to achieve the increased contact distance. The CH_4 and C_{2-5}^0 selectivity significantly increased, but the $C_{2-5}^=$ selectivity decreased to 68%; thus, the *O/P* ratio dramatically dropped from 21.2 to 7.2. Meanwhile, the ethylene selectivity was slight increased (46%) and that of long-chain C_6^+ was decreased. These results indicated that too far spatial distance of the two components was unfavorable for the syngas conversion due to the difficulty in transferring intermediate, while the too close spatial distance may cause partial shielding of acid sites in PLS-3 zeolite[34].

Hence, the granule mixing of two components provided the most suitable spatial proximity to obtain high selectivity of $C_{2-5}^{=}$ and ethylene.

Reaction mechanism of syngas conversion catalyzed by $Zn_2Al_3O_4$/PLS-3

The investigation of coke precursors helps to understand the reaction mechanism in zeolite-catalyzed syngas conversion[25]. The carbonaceous species deposited on the spent PLS-3 catalysts were investigated by thermogravimetry (TG) [Figure 7A]. The percentage of coke deposition gradually decreased from 4.2% to 2.2% with the decrease of Al content in PLS-3 zeolite, suggesting that the weakened acidity of PLS-3 zeolite can suppress the generation of carbon deposition for the syngas conversion reaction. The soluble coke species confined in the pore channels of used PLS-3 zeolite were further analyzed by the GC-MS technique [Figure 7B]. Polymethylbenzene (PMB) species, including trimethylbenzene, tetramethylbenzene, pentamethylbenzene, hexamethylbenzene, naphthalenes, and phenanthrenes, were detected in spent catalysts, potentially serving as coke precursors that contribute to catalyst deactivation. These coke precursors were dramatically reduced over the PLS-3 zeolite with a higher Si/Al ratio, consistent with the TG result. Moreover, the oxygenate species, such as dimethylbenzaldehyde, were detected, probably related to the intermediate species of syngas conversion in PLS-3 zeolite[35], and their amounts were also decreased with increasing Si/Al ratios.

For the bifunctional catalyst of metal oxide and zeolite used in syngas conversion, the zeolite component is responsible for the transformation of intermediate into desired hydrocarbons. It is currently recognized in research that methanol is the main intermediate for the bifunctional catalytic system of $ZnAlO_x$-zeolite[5,25]. Hence, the reaction mechanism of syngas conversion over $Zn_2Al_3O_4$/PLS-3-250 was further studied by the probe reaction of methanol conversion using the *in-situ* IR spectra as shown in Figure 8. Methanol was first introduced into the wafer of PLS-3-250 zeolite under the He atmosphere at 623 K. The stretching vibration of C–H of surface methoxy species (2,980, 2,966 and 1,455 cm^{-1}) and C–H bending vibration of $-CH_3$ (2,952 and 2,923 cm^{-1}) were observed, while the band at 2,891 cm^{-1} was related to the DME molecules hydrogen-boned to Si–OH[36]. Meanwhile, the symmetrical stretching vibration of $=CH_2$ at 1,463 and 1,417 cm^{-1} and the C–H vibration of olefin species at 2,876, 2,855 and 2,817 cm^{-1} were observed[25,37]. The negative bands at 3,500-3,800 cm^{-1} were related to the interaction of hydrocarbon species with hydroxyl-stretching (-OH) groups[25]. We found that the intensity of signals corresponding to olefin species at 2,876, 2,855 and 2,817 cm^{-1} slightly increased from 0 to 10 min. In the same time range, those bands corresponding to acetate species (1,544, 1,550 and 1,574 cm^{-1}) and carbonate species (1,516 and 1,508 cm^{-1}) were observed over the PLS-3 zeolite for the methanol conversion under the He [Figure 8B][16]. The bands at 1,716 and 1,768 cm^{-1} related to the C=O asymmetric vibrations in methyl acetate (MA)[38,39], and the C=O vibrations of AA at 1,744 and 1,730 cm^{-1} and acetyl at 1,704 cm^{-1} also were observed[38,40]. The intensity of the bands related to acetate, carbonate, MA, AA, and acetyl species kept increasing over time until a steady state was reached after 10 min of methanol conversion, but their intensity is relatively low under the He flow. These species were considered as key intermediates supporting the main carbonylation mechanism in methanol conversion reactions over the PLS-3 zeolite, but the hydrocarbon pool mechanism of MTO may also exist in this process[41]. Once CO/H_2 was introduced into the system to replace He after 10 min, the bands related the vibrations of gaseous CO were observed at 2,181 and 2,115 cm^{-1} over PLS-3-250 zeolite at 623 K[2,25]. Importantly, the intensity of bands corresponding to acetate, carbonate, MA, AA, and acetyl species significantly increased with the introduction of syngas, which is due to CO insertion into the methoxy group for promoting formation of these intermediates[36]. Furthermore, these key intermediates could be transformed to ethanol by hydrogenation reaction, and then ethanol further undergoes dehydration to obtain the ethylene over the PLS-3 zeolite[16].

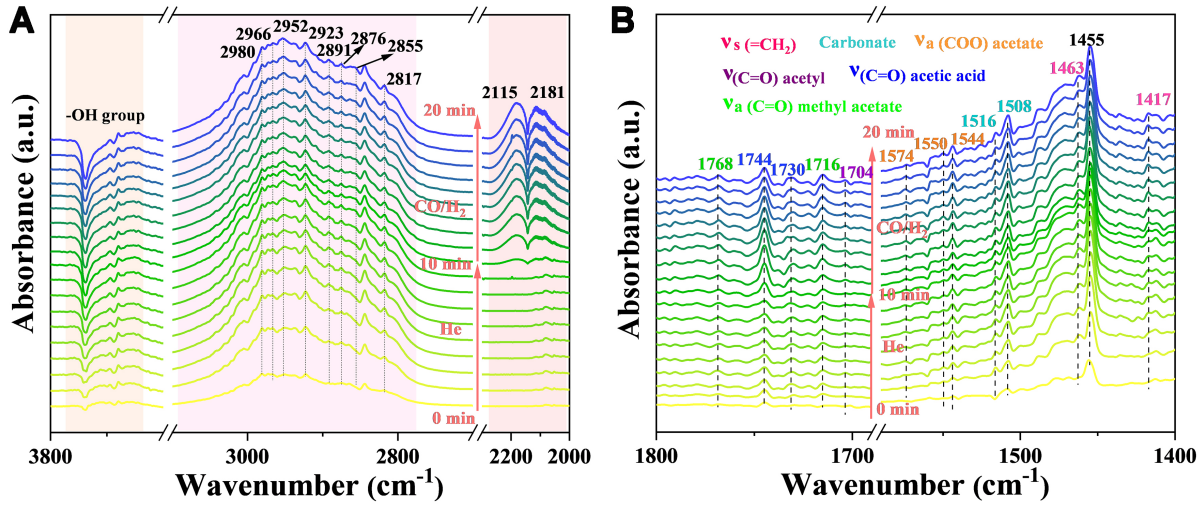

Figure 8. *In-situ* FTIR spectra when gas-phase methanol was introduced to PLS-3-250 zeolite under the He or syngas flow at temperature of 623 K. Methanol was continuously brought into *in-situ* chamber under He flow for 10 min, and then under syngas flow for another 10 min. (A) Enlarge view of the region at 3,800-2,000 cm^{-1}; (B) Enlarge view of the region at 1,800-1,400 cm^{-1}. FTIR: Fourier transform infrared spectroscopy.

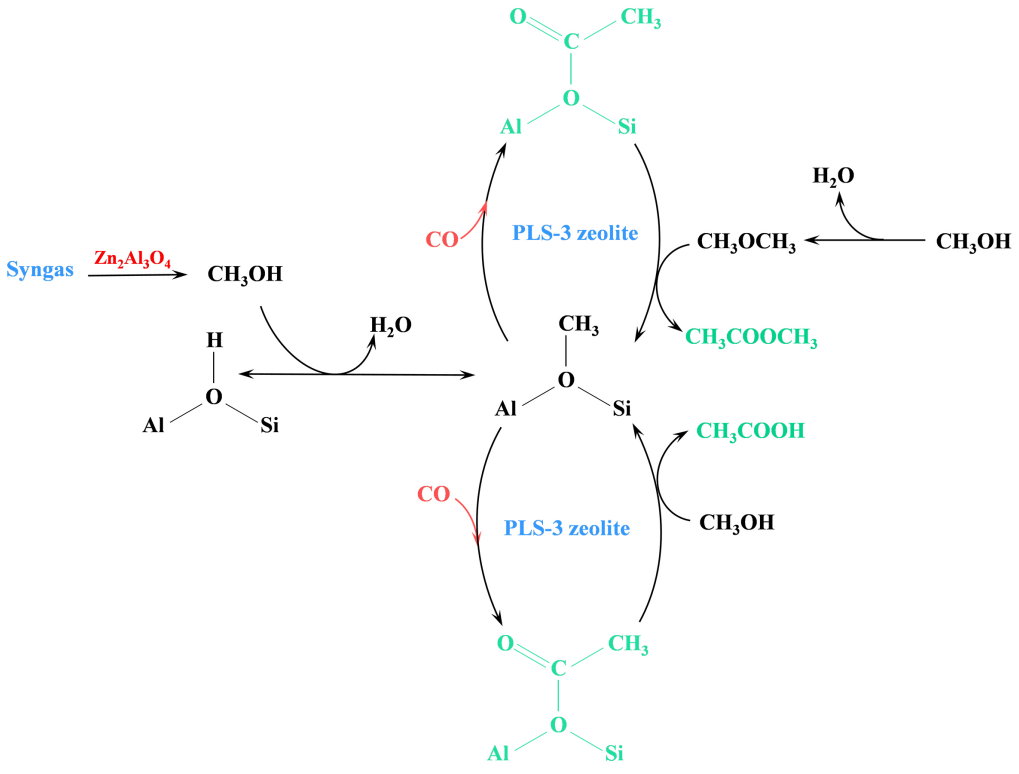

Scheme 1. Possible formation routes of key intermediates in the syngas conversion reaction over $Zn_2Al_3O_4$/PLS-3 catalyst.

Based on the above results, we propose a possible formation mechanism of key intermediates in the syngas conversion over the bifunctional $Zn_2Al_3O_4$/PLS-3 catalyst. As shown in Scheme 1, methanol carbonylation is the dominant route to form olefins (especially ethylene) for the PLS-3 zeolite with FER topology. The syngas is activated to generate the methanol/methoxy intermediate over $Zn_2Al_3O_4$ oxide[5]. Subsequently, the

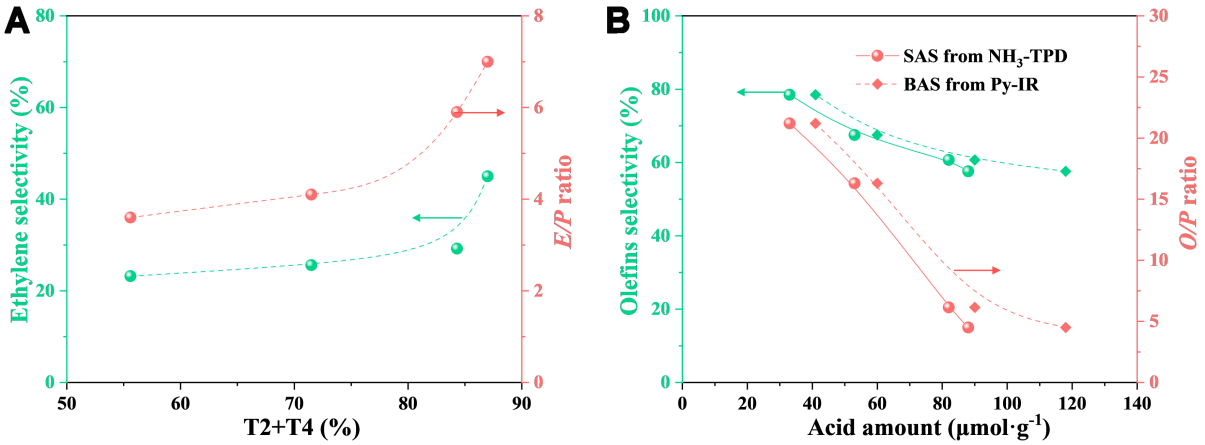

Figure 9. (A) Dependence of ethylene selectivity and *E/P* ratio on the proportion of (T2 + T4) sites; and (B) relationship between the olefin selectivity or *O/P* ratio and the acid amount. The (T2 + T4) site proportion was obtained from the ^{27}Al MAS NMR spectra. The acid amount was measured by Py-IR and NH_3-TPD techniques. *E/P*: Ethylene to propylene; *O/P*: olefin to paraffin; MAS NMR: magic angle spinning nuclear magnetic resonance; Py-IR: pyridine-adsorption infrared spectroscopy; TPD: temperature-programmed desorption.

acetyl group is converted into a methoxy group by insertion of CO over the acidic Si–OH–Al groups of PLS-3 zeolite. The formed MA and AA species are further converted into ethylene, and then longer-chain olefins (such as propylene, butene, and pentene) are formed by the oligomerization of ethylene. The previous study has indicated that the T2/T4 sites in FER are beneficial to the insertion of CO into the surface methoxy group to produce acetyl species for promoting the carbonylation reaction[26]. In this work, the proportion of Al in T2/T4 sites gradually raised with Si/Al ratios of PLS-3 zeolite as evidenced by ^{27}Al MAS NMR investigation [Supplementary Figure 3 and Table 2]. Figure 9A showed that the ethylene selectivity and *E/P* ratio gradually increased with the proportion of T2 and T4 acid sites over the PLS-3 zeolite. Hence, we speculated that the T2 and T4 sites are the main active centers, contributing to the carbonylation route in $Zn_2Al_3O_4$/PLS-3-catalyzed syngas conversion reaction. Moreover, the olefin selectivity and *O/P* ratio also gradually increased with the decreasing acid amount in PLS-3 as measured by Py-IR spectra and NH_3-TPD curves [Figure 9B]. The result indicated that weakened acidity favors the formation of olefins by suppressing the hydrogen transfer reactions to form the alkanes. Hence, the high *E/P* and *O/P* ratios are presumably attributed to two main reasons: the suitable acid site distribution and acid density of PLS-3 zeolite, which are achieved by tuning the Si/Al ratio.

CONCLUSIONS

FER-type high silica PLS-3 zeolites with nanorod crystals and tunable acidity are applied to construct bifunctional syngas conversion catalysts for selective production of olefins by combining with the $Zn_2Al_3O_4$ oxide. The acid site distribution and acidity density of PLS-3 zeolite were achieved by tuning the Si/Al ratio from 50 to 300. The decreased acid amount of PLS-3 zeolite with lower Al content restrains the side reactions (such as hydrogen transfer and aromatization reactions) and the carbon deposition, while insufficient acid sites lead to decreased catalytic performance due to difficulty in transforming methanol intermediates. Furthermore, MA, AA and acetyl intermediates were observed in $Zn_2Al_3O_4$/PLS-3-catalyzed syngas conversion reaction via the *in-situ* IR spectra, indicating the methanol carbonylation was identified as the dominant route. Meanwhile, a higher proportion of framework Al located in T2 and T4 sites of PLS-3 zeolite at low Al content favored the formation of ethylene by promoting the carbonylation route. Precisely controlling the acid property of PLS-3 zeolite allows the achievement of selective formation of olefins, providing the highest $C_{2-5}^{=}$ selectivity of 78.5%, especially high ethylene selectivity of 45.0%, and high *E/P*

(7.0) and *O/P* (21.2) ratios. This work provides a highly efficient zeolite catalyst for the conversion of syngas to olefins and proposes carbonylation mechanism for syngas conversion over oxide-zeolite bifunctional catalytic system.

DECLARATIONS

Authors' contributions

Conception and design of the study: Xu, H.; Wu, P.
Data collection and analysis: Tuo, J.
Sample preparation: Tuo, J.; Gong, X.; Yang, Q.; Sheng, Z.; Guan, Y.
Paper writing and review: Tuo, J.; Xu, H.; Wu, P.

Availability of data and materials

The detailed materials and methods in the experiment were listed in the Supplementary Materials. Other raw data that support the findings of this study are available from the corresponding author upon reasonable request.

Financial support and sponsorship

We gratefully acknowledge the financial support from NSFC of China (Grant Nos. 22222201 and 22272054) and the National Key Research and Development Program of China (2023YFB3810602 and 2021YFA1501401).

Conflicts of interest

All authors declared that there are no conflicts of interest.

Ethical approval and consent to participate

Not applicable.

Consent for publication

Not applicable.

REFERENCES

1. Han, Q.; Gao, P.; Chen, K.; et al. Synergistic interplay of dual active sites on spinel $ZnAl_2O_4$ for syngas conversion. *Chem* **2023**, *9*, 721-38. DOI
2. Lyu, S.; Wang, Y.; Qian, J.; et al. Role of residual CO molecules in OX–ZEO relay catalysis for syngas direct conversion. *ACS. Catal.* **2021**, *11*, 4278-87. DOI
3. Wang, S.; Wang, P.; Shi, D.; et al. Direct conversion of syngas into light olefins with low CO_2 emission. *ACS. Catal.* **2020**, *10*, 2046-59. DOI
4. Torres Galvis, H. M.; de Jong, K. P. Catalysts for production of lower olefins from synthesis gas: a review. *ACS. Catal.* **2013**, *3*, 2130-49. DOI
5. Ren, L.; Zhang, J.; Wang, B.; et al. Syngas to light olefins over $ZnAlO_x$ and high-silica CHA prepared by boron-assisted hydrothermal synthesis. *Fuel* **2022**, *307*, 121916. DOI
6. Torres Galvis, H. M.; Bitter, J. H.; Khare, C. B.; Ruitenbeek, M.; Dugulan, A. I.; de Jong, K. P. Supported iron nanoparticles as catalysts for sustainable production of lower olefins. *Science* **2012**, *335*, 835-8. DOI PubMed
7. Zhong, L.; Yu, F.; An, Y.; et al. Cobalt carbide nanoprisms for direct production of lower olefins from syngas. *Nature* **2016**, *538*, 84-7. DOI PubMed
8. Sun, Q.; Wang, N.; Yu, J. Advances in catalytic applications of zeolite-supported metal catalysts. *Adv. Mater.* **2021**, *33*, e2104442. DOI PubMed
9. Song, F.; Yong, X.; Wu, X.; et al. FeMn@HZSM-5 capsule catalyst for light olefins direct synthesis via Fischer-Tropsch synthesis:

Studies on depressing the CO_2 formation. *Appl. Catal. B. Environ.* **2022**, *300*, 120713. DOI
10. Qiu, T.; Wang, L.; Lv, S.; et al. SAPO-34 zeolite encapsulated Fe_3C nanoparticles as highly selective Fischer-Tropsch catalysts for the production of light olefins. *Fuel* **2017**, *203*, 811-6. DOI
11. Ni, Y.; Liu, Y.; Chen, Z.; et al. Realizing and recognizing syngas-to-olefins reaction via a dual-bed catalyst. *ACS. Catal.* **2019**, *9*, 1026-32. DOI
12. Jiao, F.; Li, J.; Pan, X.; et al. Selective conversion of syngas to light olefins. *Science* **2016**, *351*, 1065-8. DOI PubMed
13. Cheng, K.; Gu, B.; Liu, X.; Kang, J.; Zhang, Q.; Wang, Y. Direct and highly selective conversion of synthesis gas into lower olefins: design of a bifunctional catalyst combining methanol synthesis and carbon–carbon coupling. *Angew. Chem. Int. Ed. Engl.* **2016**, *55*, 4725-8. DOI PubMed
14. Wang, C.; Wang, Y.; Xie, Z. Methylation of olefins with ketene in zeotypes and its implications for the direct conversion of syngas to light olefins: a periodic DFT study. *Catal. Sci. Technol.* **2016**, *6*, 6644-9. DOI
15. Pan, X.; Jiao, F.; Miao, D.; Bao, X. Oxide-zeolite-based composite catalyst concept that enables syngas chemistry beyond Fischer-Tropsch synthesis. *Chem. Rev.* **2021**, *121*, 6588-609. DOI PubMed
16. Chen, K.; Wang, F.; Wang, Y.; et al. Relay catalysis for highly selective conversion of methanol to ethylene in syngas. *JACS. Au.* **2023**, *3*, 2894-904. DOI PubMed PMC
17. Zhu, Y.; Pan, X.; Jiao, F.; et al. Role of manganese oxide in syngas conversion to light olefins. *ACS. Catal.* **2017**, *7*, 2800-4. DOI
18. Liu, X.; Zhou, W.; Yang, Y.; et al. Design of efficient bifunctional catalysts for direct conversion of syngas into lower olefins *via* methanol/dimethyl ether intermediates. *Chem. Sci.* **2018**, *9*, 4708-18. DOI PubMed PMC
19. Su, J.; Zhou, H.; Liu, S.; et al. Syngas to light olefins conversion with high olefin/paraffin ratio using $ZnCrO_x$/AlPO-18 bifunctional catalysts. *Nat. Commun.* **2019**, *10*, 1297. DOI PubMed PMC
20. Li, G.; Jiao, F.; Pan, X.; et al. Role of SAPO-18 acidity in direct syngas conversion to light olefins. *ACS. Catal.* **2020**, *10*, 12370-5. DOI
21. Su, J.; Zhang, L.; Zhou, H.; et al. Unveiling the anti-trap effect for bridging intermediates on $ZnAlO_x$/AlPO-18 bifunctional catalysts to boost syngas to olefin conversion. *ACS. Catal.* **2023**, *13*, 2472-81. DOI
22. Wang, M.; Kang, J.; Xiong, X.; et al. Effect of zeolite topology on the hydrocarbon distribution over bifunctional ZnAlO/SAPO catalysts in syngas conversion. *Catal. Today.* **2021**, *371*, 85-92. DOI
23. Jiao, F.; Pan, X.; Gong, K.; Chen, Y.; Li, G.; Bao, X. Shape-selective zeolites promote ethylene formation from syngas via a ketene intermediate. *Angew. Chem. Int. Ed. Engl.* **2018**, *57*, 4692-6. DOI PubMed
24. Jiao, F.; Bai, B.; Li, G.; et al. Disentangling the activity-selectivity trade-off in catalytic conversion of syngas to light olefins. *Science* **2023**, *380*, 727-30. DOI PubMed
25. Tuo, J.; Fan, Y.; Wang, Y.; et al. Promoting syngas to olefins with isolated internal silanols-enriched Al-IDM-1 aluminosilicate nanosheets. *Angew. Chem. Int. Ed. Engl.* **2023**, *62*, e202313785. DOI PubMed
26. Tuo, J.; Wang, J.; Gong, X.; et al. Ferrierite nanosheets with preferential Al locations as catalysts for carbonylation of dimethyl ether. *Fuel* **2024**, *357*, 130001. DOI
27. Dai, W.; Ruaux, V.; Deng, X.; et al. Synthesis and catalytic application of nanorod-like FER-type zeolites. *J. Mater. Chem. A.* **2021**, *9*, 24922-31. DOI
28. Yang, B.; Jiang, J.; Xu, H.; Liu, Y.; Peng, H.; Wu, P. Selective skeletal isomerization of 1-butene over FER-type zeolites derived from PLS-3 lamellar precursors. *Appl. Catal. A. Gen.* **2013**, *455*, 107-13. DOI
29. Tuo, J.; Lv, J.; Fan, S.; et al. One-pot synthesis of [Mn,H]ZSM-5 and the role of Mn in methanol-to-propylene reaction. *Fuel* **2022**, *308*, 121995. DOI
30. Tuo, J.; Fan, S.; Yang, N.; et al. Direct synthesis of [B,H]ZSM-5 by a solid-phase method: Al_F siting and catalytic performance in the MTP reaction. *Catal. Sci. Technol.* **2020**, *10*, 7034-45. DOI
31. Liu, R.; Zeng, S.; Sun, T.; et al. Selective removal of acid sites in mordenite zeolite by trimethylchlorosilane silylation to improve dimethyl ether carbonylation stability. *ACS. Catal.* **2022**, *12*, 4491-500. DOI
32. Gong, Y.; Tuo, J.; Li, S.; et al. Direct synthesis of IDM-1 aluminosilicate nanosheets with improved MTP performance. *Chem. Commun.* **2023**, *59*, 724-7. DOI PubMed
33. Li, S.; Peng, R.; Wan, Z.; et al. A nanostrips-assemble morphology of ZSM-5 zeolite for efficient propylene production from methanol conversion. *ACS. Sustain. Chem. Eng.* **2023**, *11*, 10274-83. DOI
34. Ding, Y.; Jiao, F.; Pan, X.; et al. Effects of proximity-dependent metal migration on bifunctional composites catalyzed syngas to olefins. *ACS. Catal.* **2021**, *11*, 9729-37. DOI
35. Xie, M.; Fang, X.; Liu, H.; et al. Cyclic oxygenate-based deactivation mechanism in dimethyl ether carbonylation reaction over a pyridine-modified H-MOR catalyst. *ACS. Catal.* **2023**, *13*, 14327-33. DOI
36. Xiong, Z.; Zhan, E.; Li, M.; Shen, W. DME carbonylation over a HSUZ-4 zeolite. *Chem. Commun.* **2020**, *56*, 3401-4. DOI
37. Ma, K.; Zhao, S.; Dou, M.; Ma, X.; Dai, C. Enhancing the stability of methanol-to-olefins reaction catalyzed by SAPO-34 zeolite in the presence of CO_2 and oxygen-vacancy-rich $ZnCeZrO_x$. *ACS. Catal.* **2024**, *14*, 594-607. DOI
38. Liu, J.; Xue, H.; Huang, X.; et al. Stability enhancement of H-mordenite in dimethyl ether carbonylation to methyl acetate by pre-adsorption of pyridine. *Chin. J. Catal.* **2010**, *31*, 729-38. DOI
39. Zhou, H.; Zhu, W.; Shi, L.; et al. In situ DRIFT study of dimethyl ether carbonylation to methyl acetate on H-mordenite. *J. Mol. Catal. A. Chem.* **2016**, *417*, 1-9. DOI

40. Cheung, P.; Bhan, A.; Sunley, G.; Law, D.; Iglesia, E. Site requirements and elementary steps in dimethyl ether carbonylation catalyzed by acidic zeolites. *J. Catal.* **2007**, *245*, 110-23. DOI
41. Plessow, P. N.; Studt, F. Unraveling the mechanism of the initiation reaction of the methanol to olefins process using ab initio and DFT calculations. *ACS. Catal.* **2017**, *7*, 7987-94. DOI

Jie Tuo

Jie Tuo received his master's degree in chemical engineering in 2021 from the State Key Laboratory of High-efficiency Utilization of Coal and Green Chemical Engineering. Now he is pursuing his PhD in East China Normal University under the supervision of Prof. Peng Wu. His scientific interests focus on zeolites synthesis and CO_X catalytic conversion.

Xianchen Gong

Xianchen Gong is currently pursuing a Ph.D. at East China Normal University under the guidance of Professor Peng Wu. His research focuses on zeolite synthesis and homogeneous catalysis.

Zhenteng Sheng

Zhenteng Sheng obtained his master's degree in Physical Chemistry from South Central Minzu University in 2024. He is currently pursuing a Ph.D. at East China Normal University under the supervision of Professor Peng Wu. His research focuses on the catalytic conversion of C_1 molecules using zeolite-based materials.

Qi Yang

Qi Yang received her Master of Engineering degree from Chongqing Technology and Business University in 2023. She is currently pursuing a Ph.D. at the School of Chemistry and Molecular Engineering, East China Normal University, under the supervision of Professor Yejun Guan. Her research focuses on green chemistry and hierarchical porous materials.

Hao Xu

Hao Xu obtained her Ph.D. in Physical Chemistry from East China Normal University (ECNU) in 2014. Following a 1.5-year postdoctoral fellowship at the École Normale Supérieure de Lyon, France, she began her independent research at ECNU in 2016 and was promoted to Professor in 2021.

Her research focuses on the design, synthesis, and catalytic applications of novel zeolites. She has published over 60 papers as first or corresponding author in SCI-indexed journals. She was awarded the **Rising Star Award of Chinese Zeolite** in 2019 and the **Excellent Young Scientists Fund** from the National Natural Science Foundation of China (NSFC) in 2022.

Yejun Guan

Yejun Guan received his B.Sc. in Chemistry from Shaanxi Normal University in 2000 and his Ph.D. in Physical Chemistry from the State Key Laboratory of Catalysis, Dalian Institute of Chemical Physics, in 2007. He conducted four years of postdoctoral research at TU Eindhoven and the University of Twente before joining East China Normal University as an Associate Professor in 2011. He was promoted to Full Professor in 2020.

His current research focuses on the rational design of zeolite-supported metal nanoparticles and their applications in C_1 chemistry, the conversion of biomass-derived platform compounds, and hydrocarbon transformations. He has published over 100 peer-reviewed articles as a co-author or corresponding author in journals such as *Nature Catalysis*, *Applied Catalysis B: Environmental*, *ACS Catalysis*, *Journal of Catalysis*, *Chinese Journal of Catalysis*, *Green Chemistry*, *ChemSusChem*, *Chemistry - A European Journal*, and others. His work has earned him an H-index of 30.

Peng Wu

Peng Wu is a Professor and Ph.D. supervisor at the School of Chemistry and Molecular Engineering, East China Normal University. He also serves as an editor for *Microporous and Mesoporous Materials* and the *Chinese Journal of Catalysis*.

His research focuses on zeolite-based heterogeneous catalytic materials and green catalytic processes. His interests include the design and synthesis of catalysts for selective hydrocarbon oxidation and the development of environmentally friendly chemical technologies.

Professor Wu has received the **National Science Fund for Distinguished Young Scholars** from the National Natural Science Foundation of China and has been recognized by several prestigious national and regional talent programs. These include the **Changjiang Scholars Program** (Ministry of Education), the **National New Century Talents Project**, the **New Century Excellent Talents Program** (Ministry of Education), the **Shanghai Oriental Scholars Program**, the **Pujiang Talent Program**, the **Outstanding Academic Leader Program**, and the **Leading Talent Program of Shanghai**.

He has published over 300 research papers in peer-reviewed academic journals.